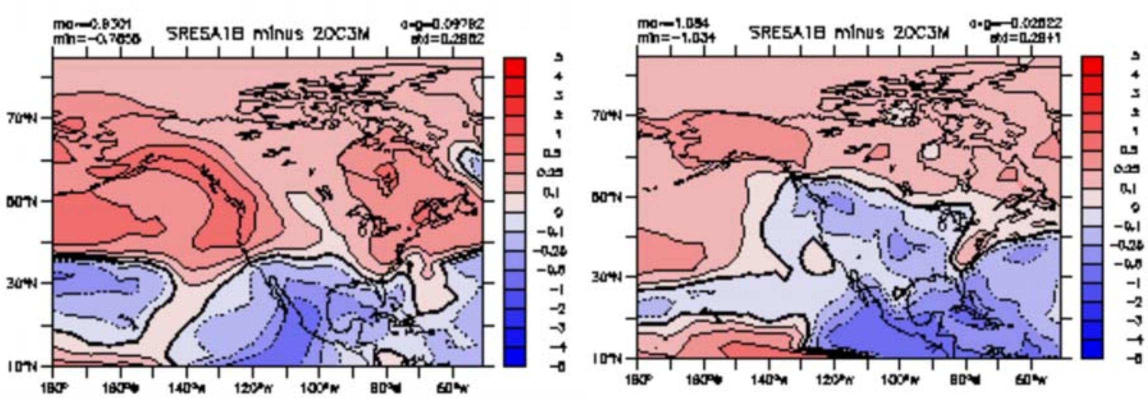

Figure 11.3.5.5. Ensemble-mean projected DJF and JJA fractional precipitation changes from AR4 CGCMs (fraction of precipitation)

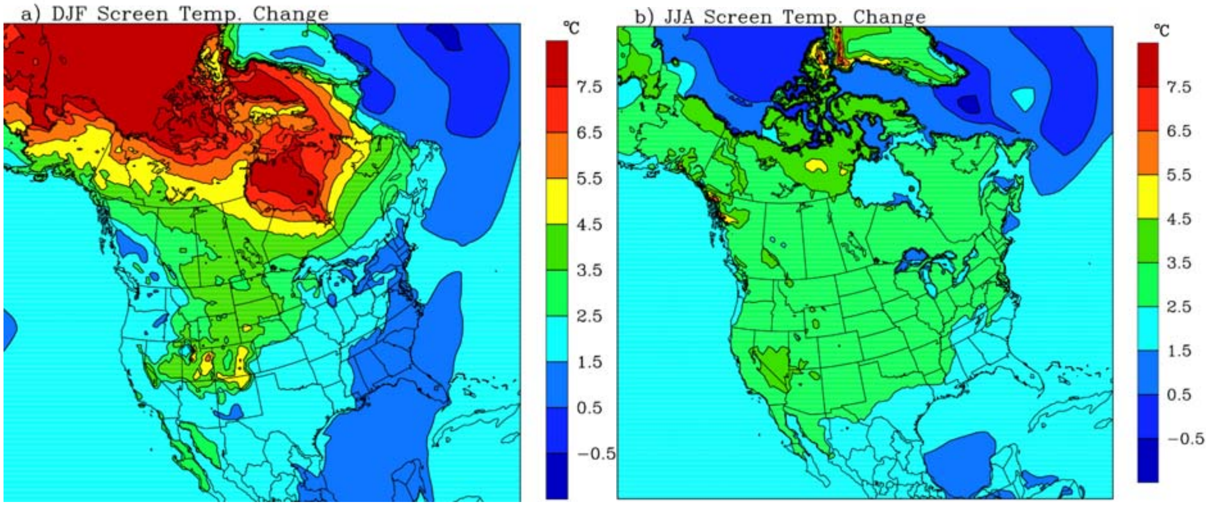

Figure 11.3.5.6. Ensemble-mean projected DJF and JJA surface air temperature change, (2041–2070) minus (1961–1990), from 3 pairs of realisations with 2 variants of CRCM_3 nested by CGCM2 under 2 SRES, scenarios, IS92a and A2 (from Plummer et al., 2006)

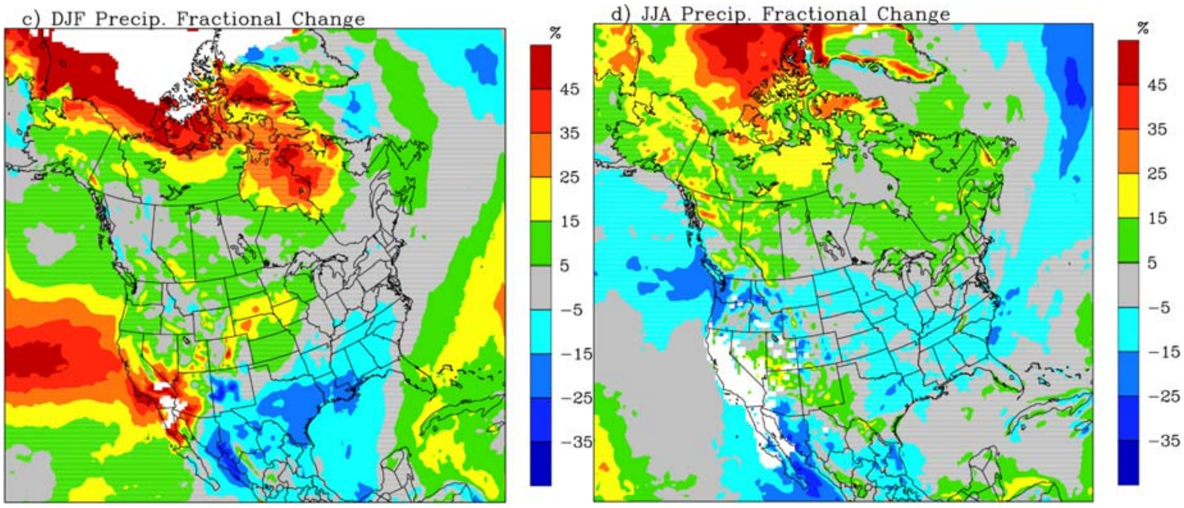

Figure 11.3.5.7. Ensemble-mean projected DJF and JJA precipitation fractional, (2041–2070) minus (1961–1990), from 3 pairs of realisations with 2 variants of CRCM_3 nested by CGCM2 under 2 SRES, scenarios, IS92a and A2 (from Plummer et al., 2006) (NB The white areas correspond to cases when the denominator is less than 0.25 mm/day, in which case the fractions are not computed)

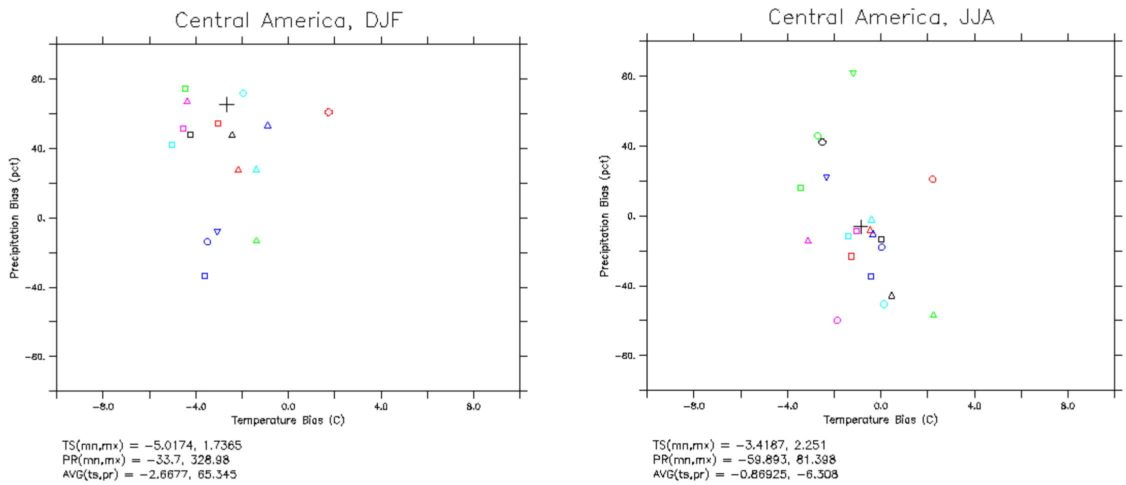

Figure11.3.6.1. Model biases in temperature and precipitation for the Mesoamerican region determined from the A1B AR4 experiments. a) for December-January-February and b) for June-July-August.

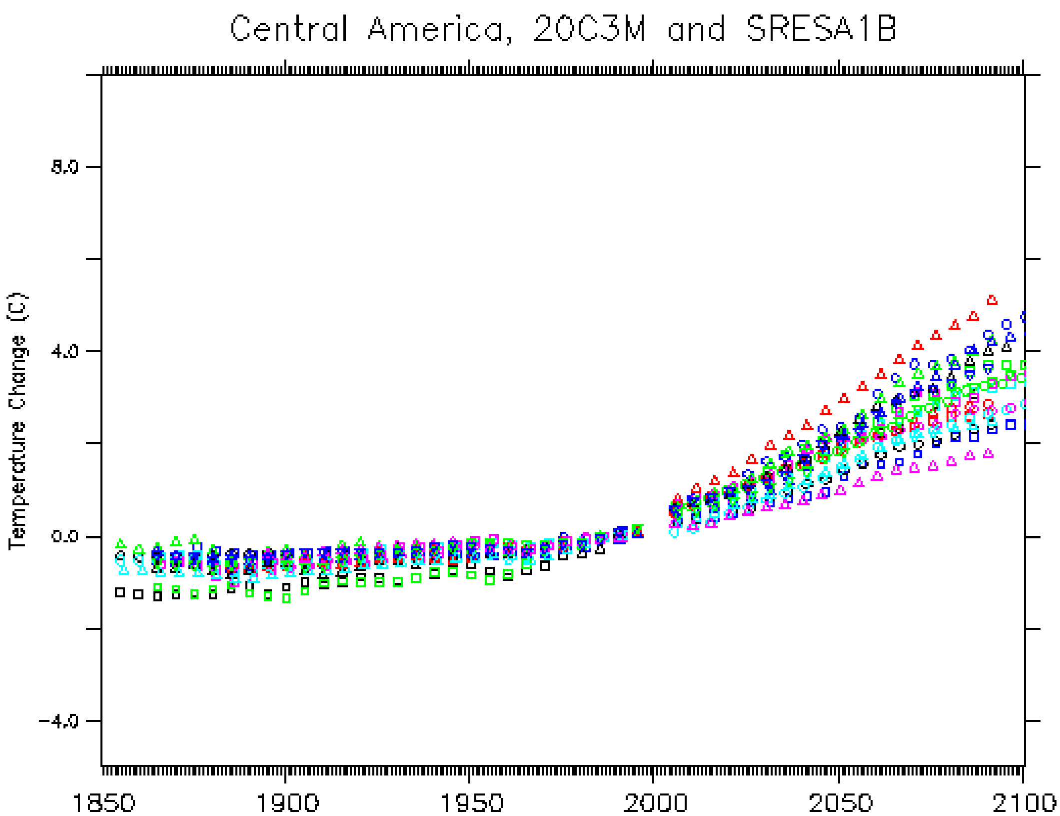

Figure11.3.6.2. Surface temperature difference between the annual mean climatology from the A1B AR4 ensamble experiments and the control 20th century climatology over Mesoamerica.

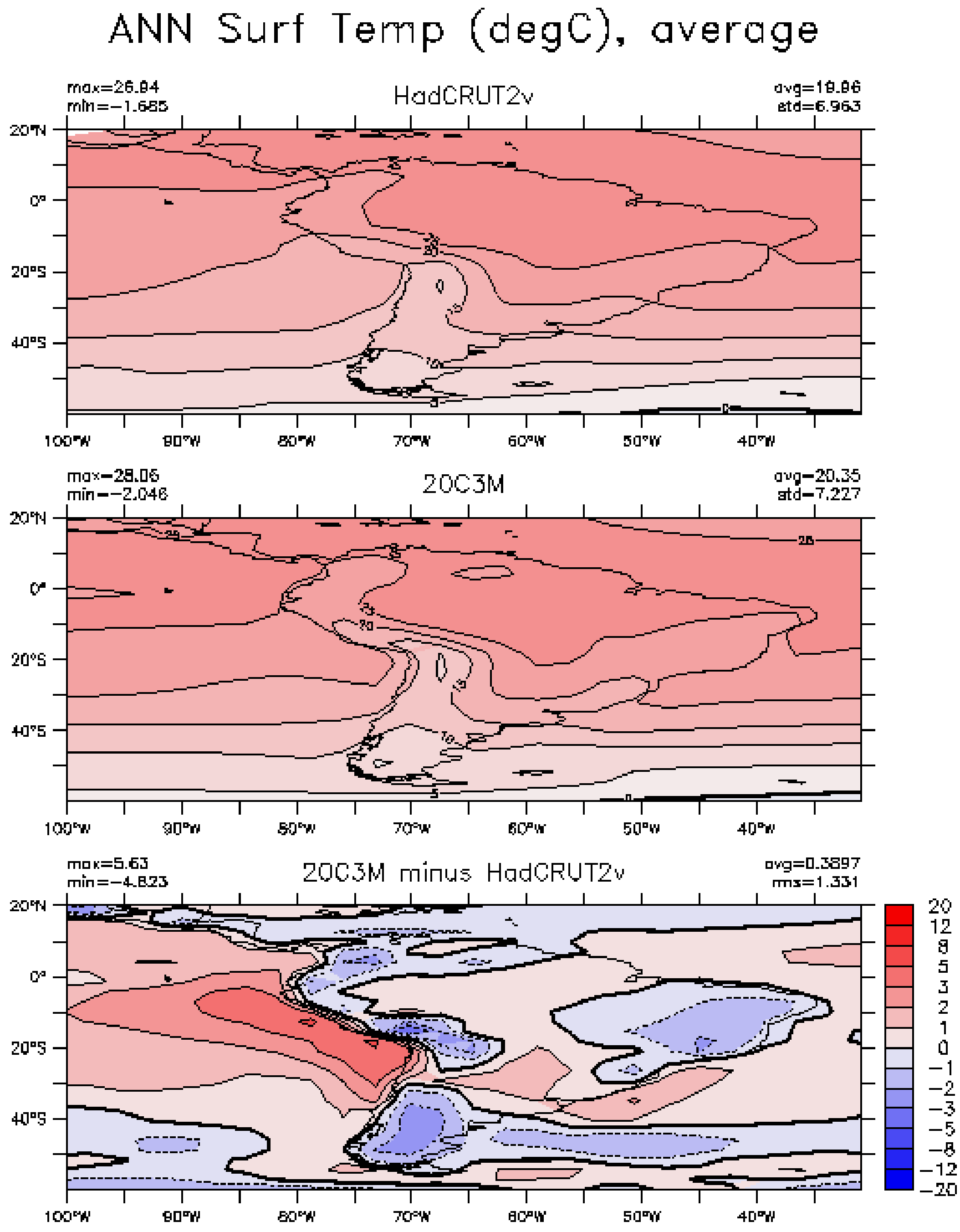

Figure11.3.6.3. AR4 Ensemble annual mean temperatures compared with obsertion. a) observed from the Hadley Centre; b) model mean; c) model mean bias. Units °C

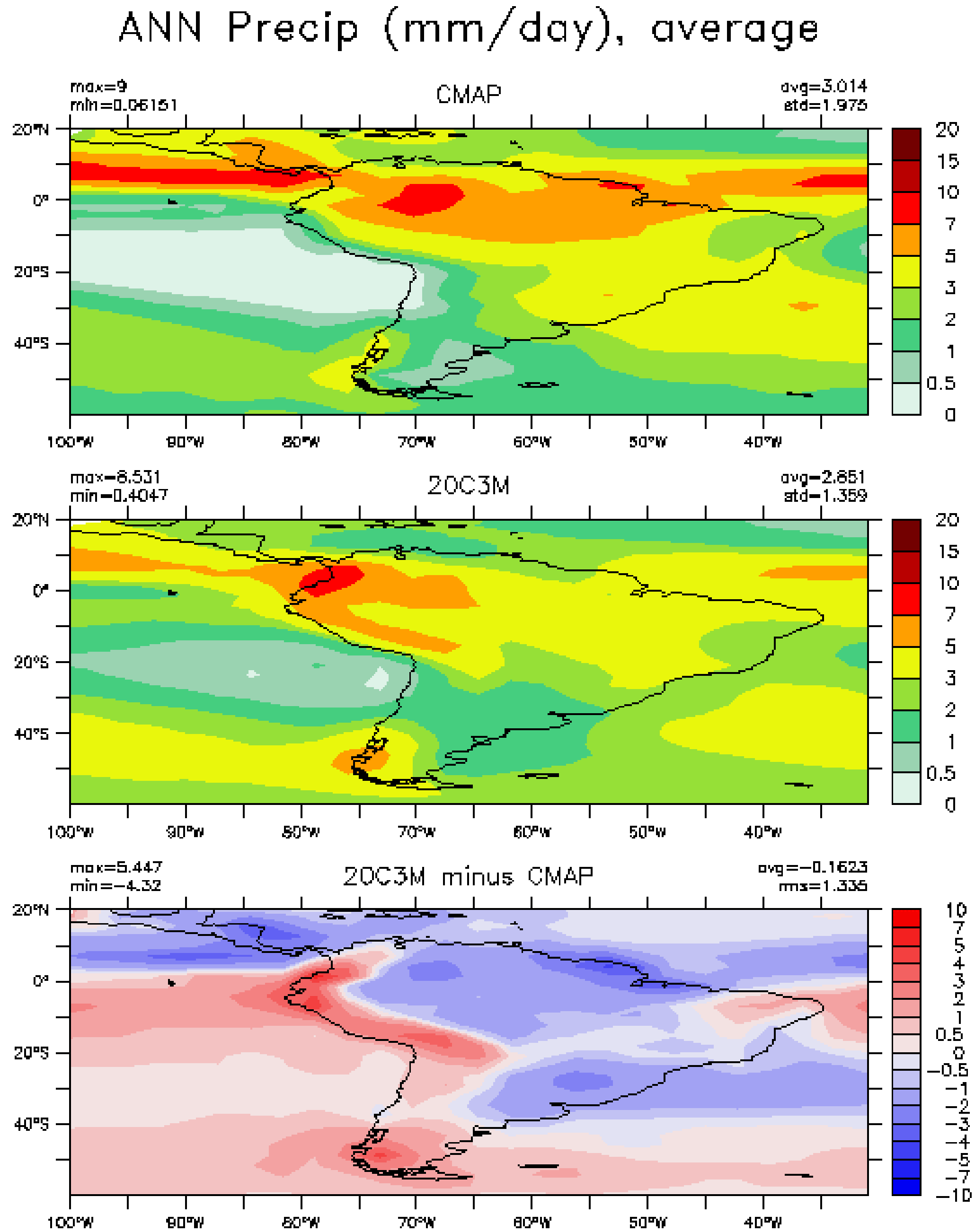

Figure11.3.6.4. As Figure 11.3.6.3, but for precipitation. Observations CMAP. Units mm/day

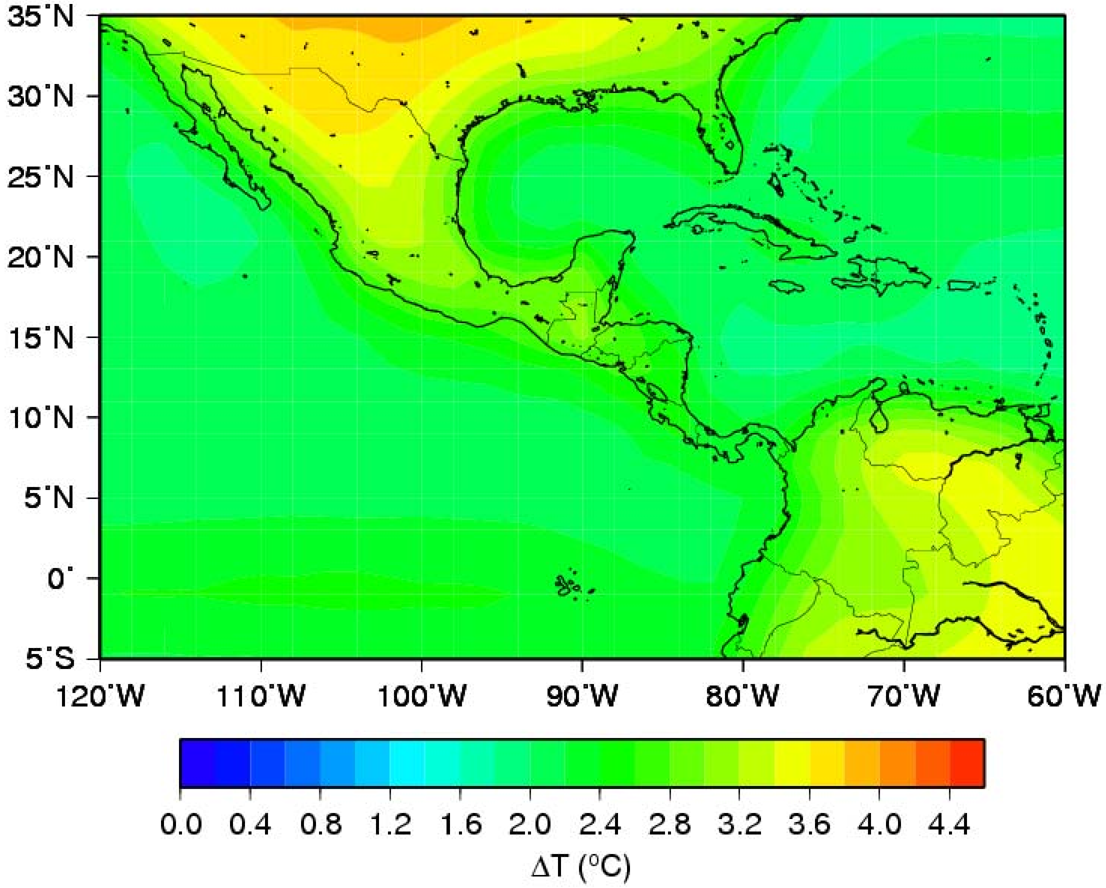

Figure11.3.6.5. Surface temperature difference between the annual mean for the 2070–2099 climatology from the AR4 ensamble experiments and the 20th century climatology.

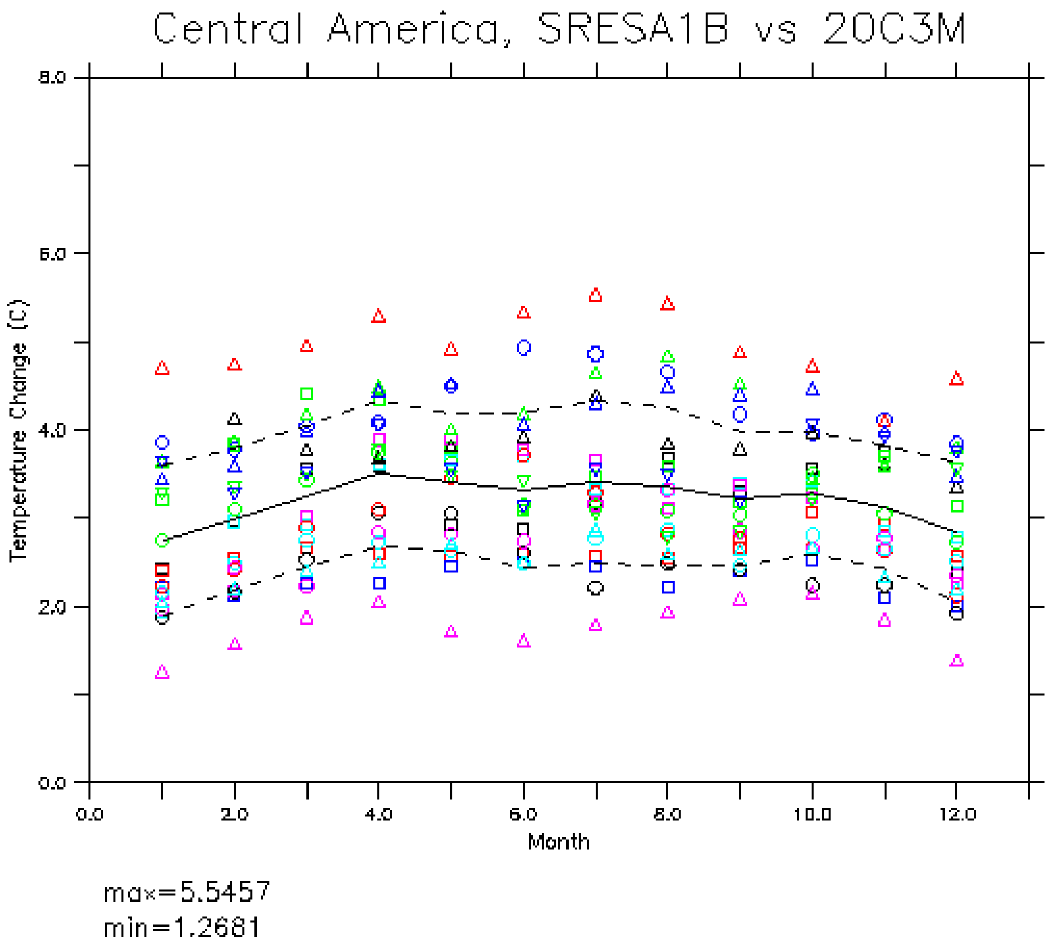

Figure11.3.6.6. Monthly distribution of the surface temperature differences from the A1B AR4 experiments and the 20th century climatology in the Mesoamerican region. Solid line corresponds to the mean value.

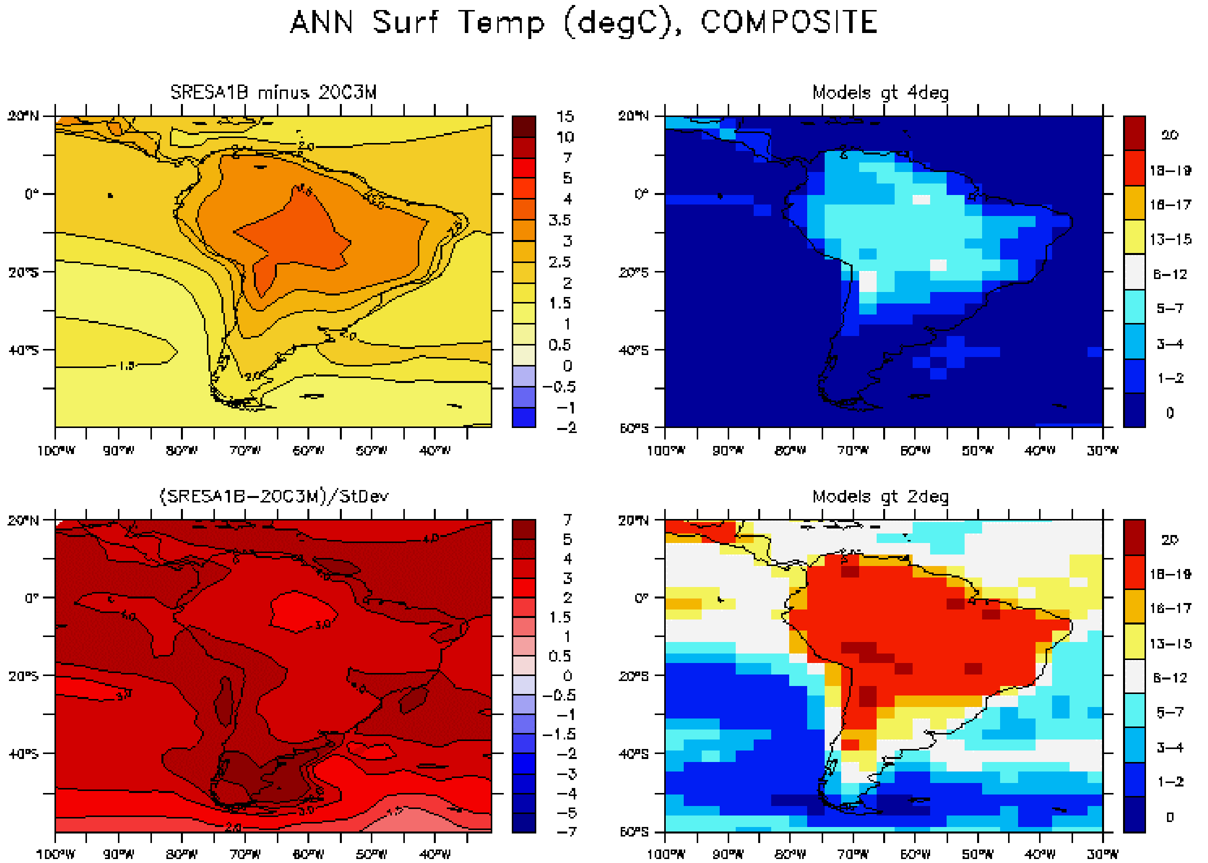

Figure11.3.6.7. AR4 Annual mean temperature temperature change. a) ensembles mean; b); signal to noise ratio; c) number of models with a temperature increase above 4°C; d) number of models with a temperature increase above 2°C

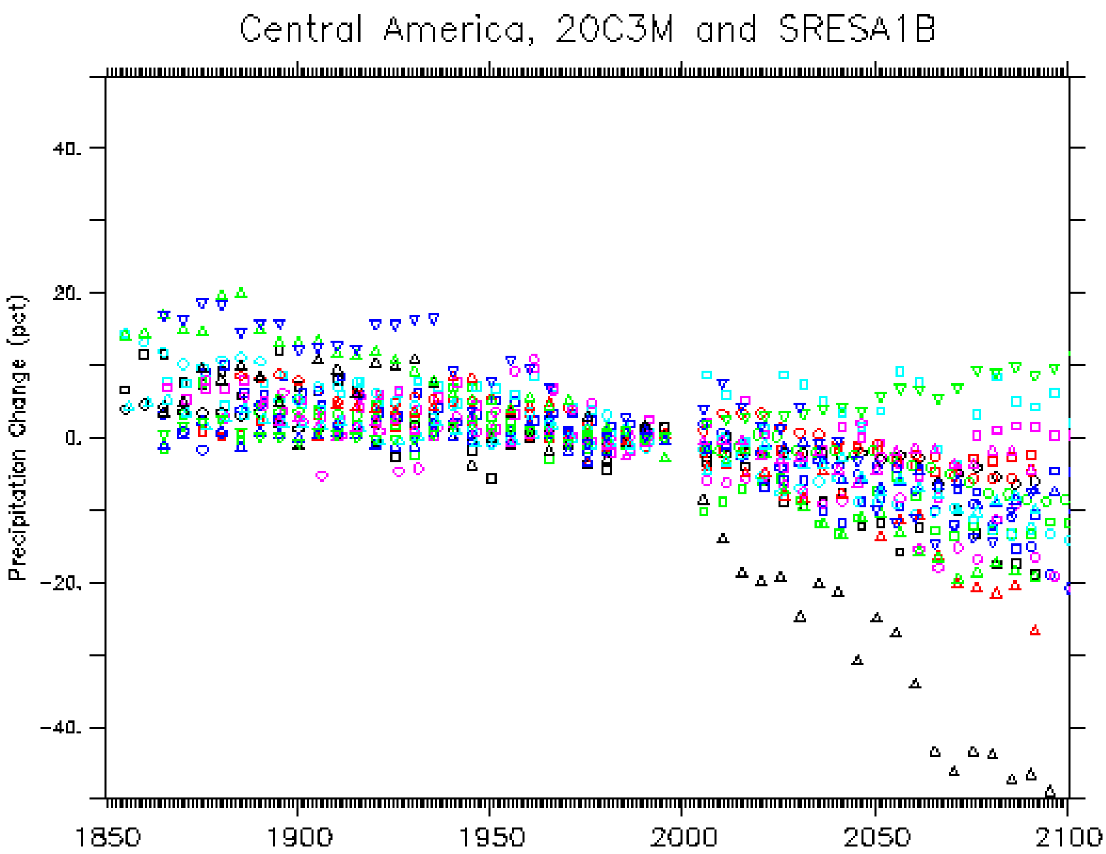

Figure11.3.6.8. As in Figure 11.3.6.2 but for precipitation

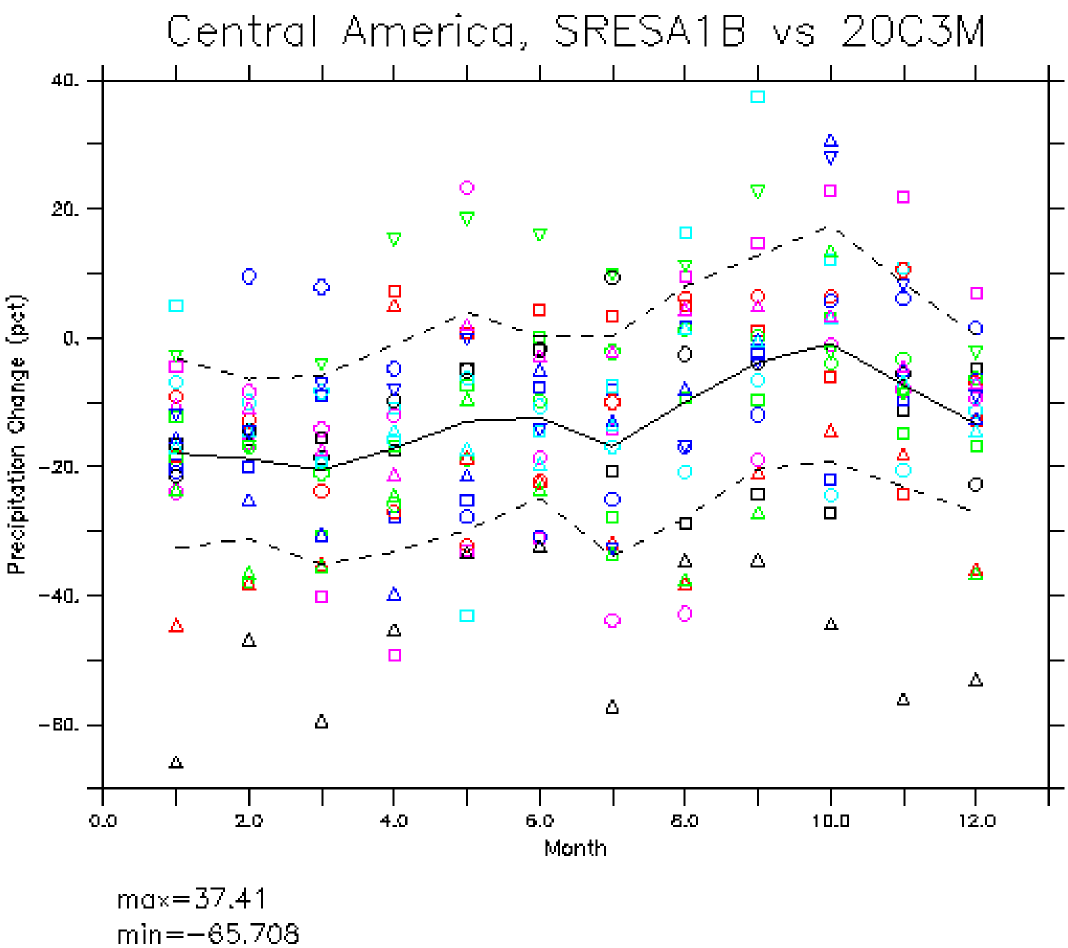

Figure11.3.6.9. As in Figure11.3.6.6 but for precipitation

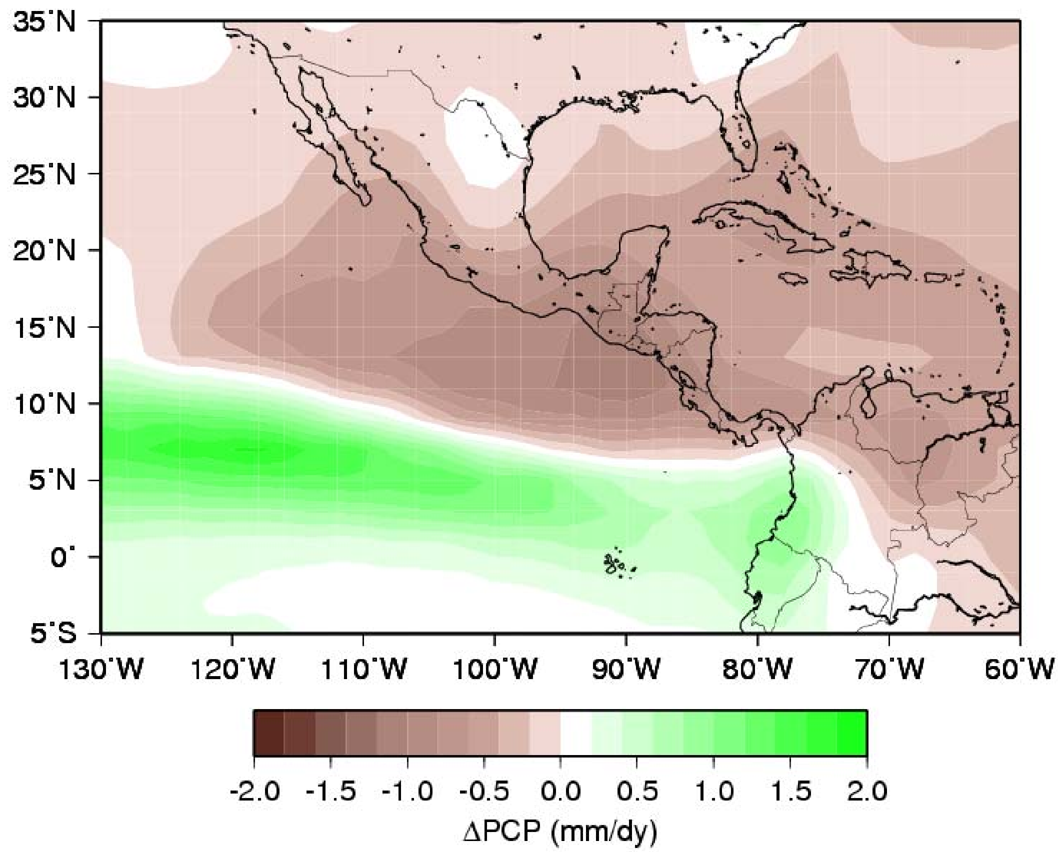

Figure11.3.6.10. As in Figure 11.3.6.5 but for June-July-August precipitation.

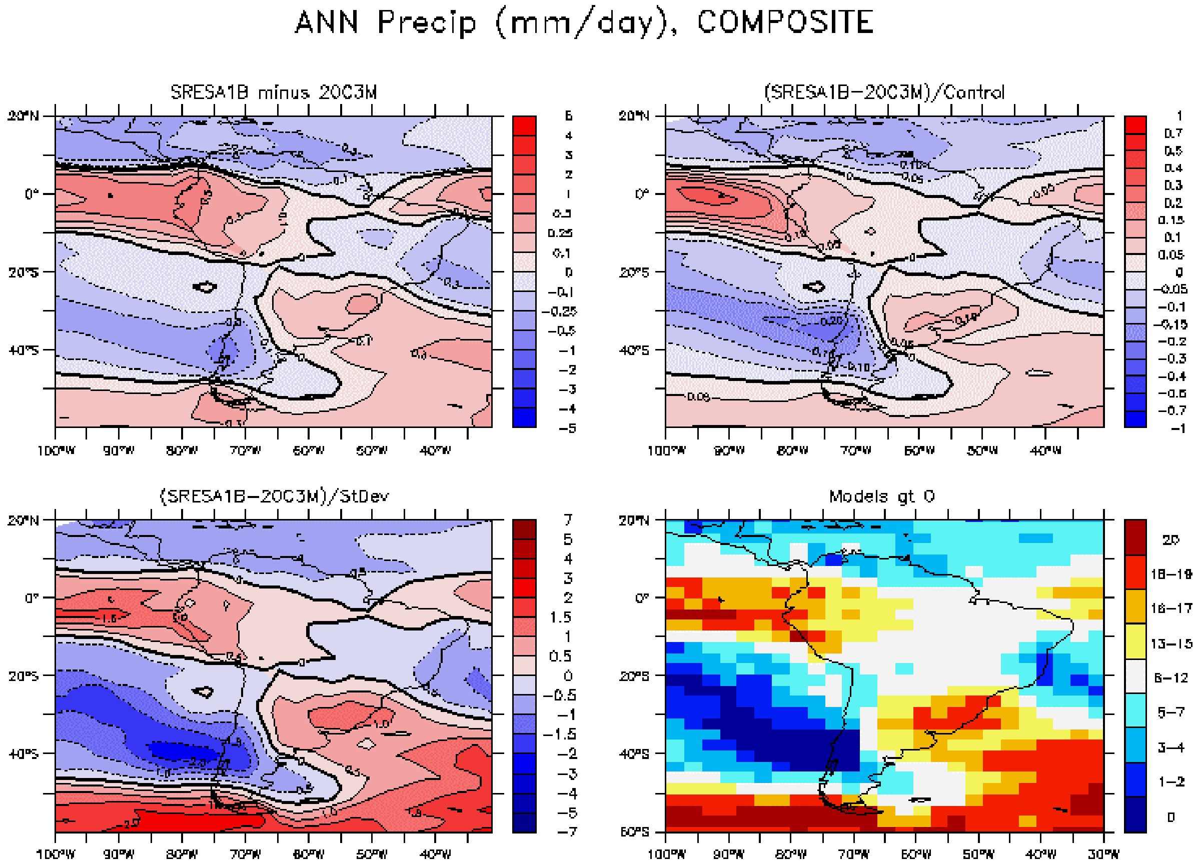

Figure11.3.6.11. Robustness of climate change precipitation response from models in the AR4/PCMDI archive. Top panel shows the annual precipitation anomaly between 2079–2099 and 1979–1999 periods – absolute (left) and relative (right). The lower panel shows the signal to noise of the projected change and the number of models (out of 20) that predict mositening at a given location.

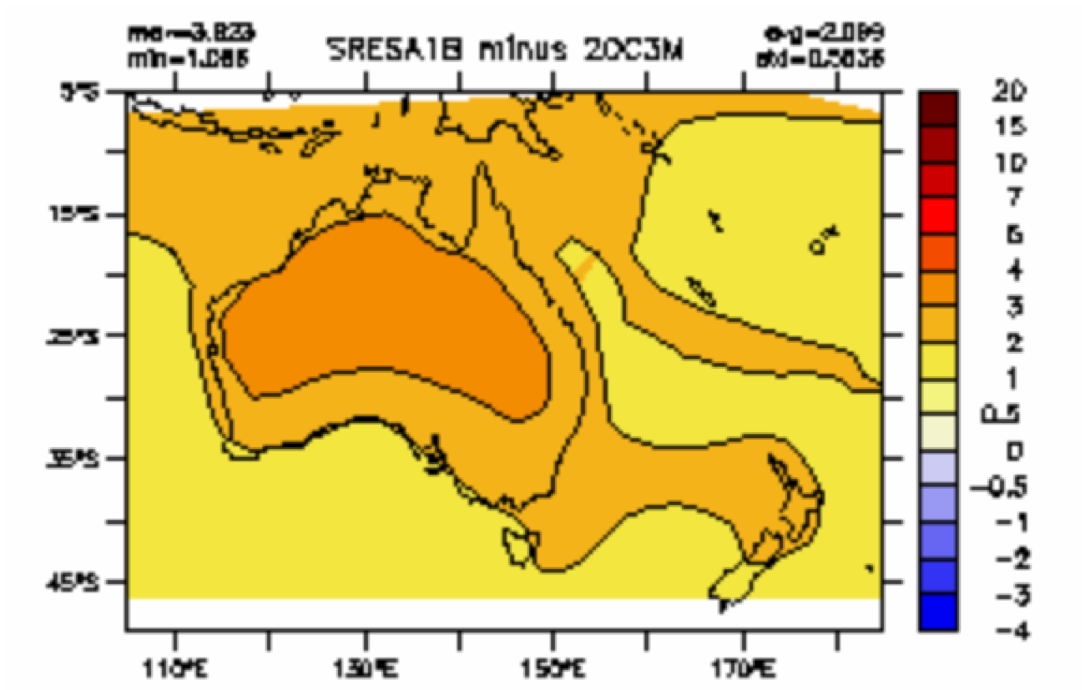

Figure 11.3.7.1. Annual mean warming (surface air temperature1979–1998 to 2079–2098) in A1B averaged over all AR4 simulations. [To be redrawn with increased contour interval]

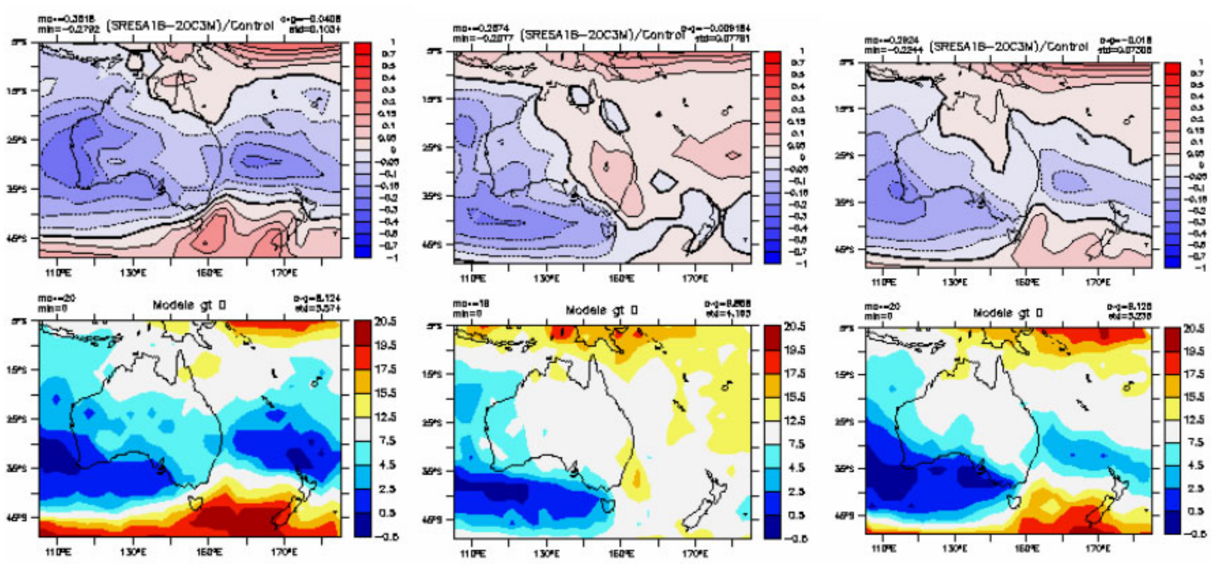

Figure 11.3.7.2. Upper panels: fractional change in precipitation (left-to-right: JJA, DJF, ANN) 1979–1998 to 2079–2098 in A1B averaged over all AR4 simulations. Lower panels, number of models projecting increase in precipitation. [To be redrawn]

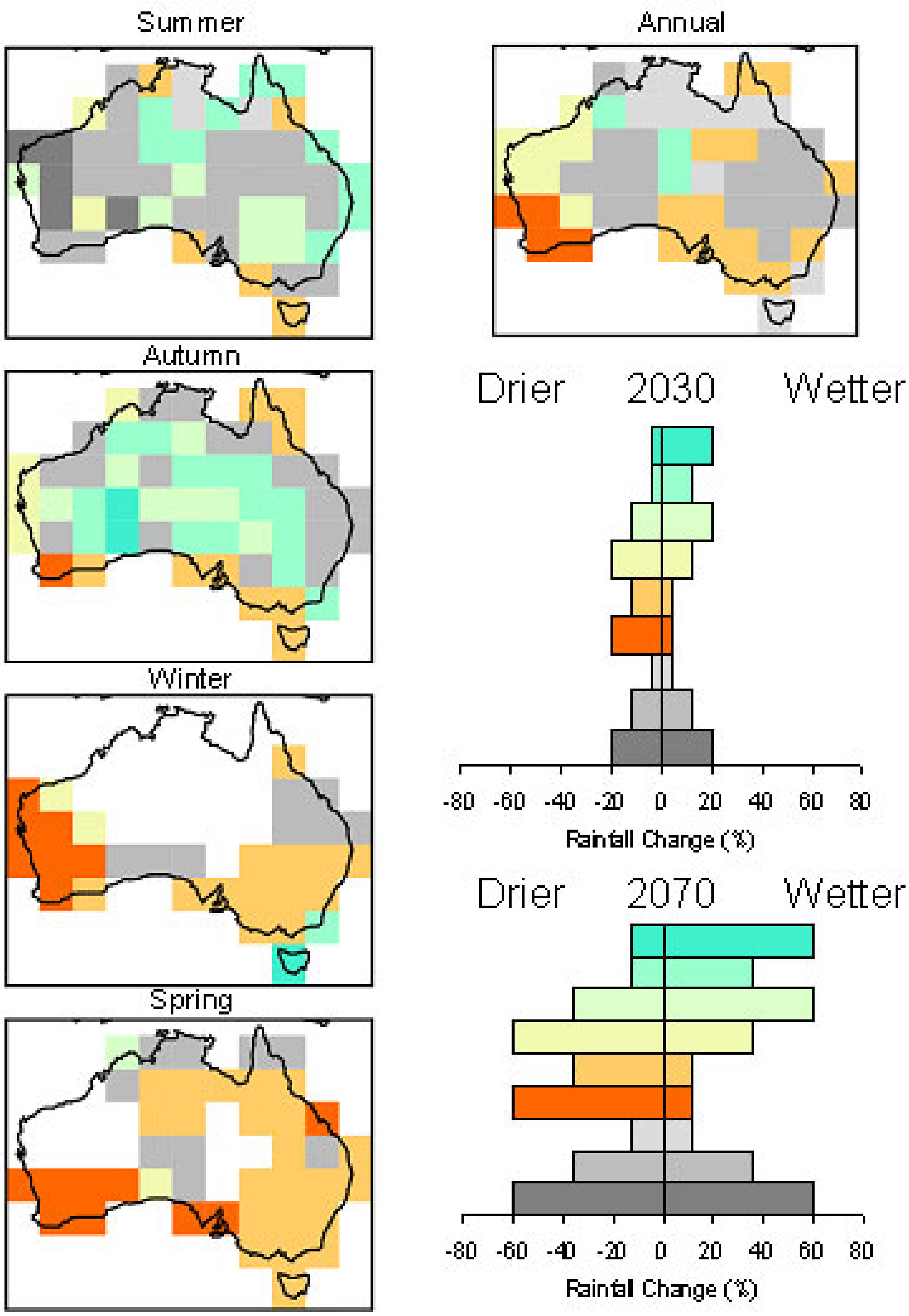

Figure 11.3.7.3. Ranges of average seasonal and annual rainfall change (%) for around 2030 and 2070 relative to 1990. The coloured bars show the ranges of change for areas with corresponding colours in the maps. The range of uncertainty represented by the coloured bar is due to uncertainty in global warning at the given date (as in IPCC, 2001) and differences in regional response (% change per degree of global warming) in the eight AOGCMs and one regional model used. Ranges are not given for areas with seasonally low rainfall because percentage changes in rainfall cannot be as readily calculated or applied in such regions. Source: CSIRO, 2001. *[to be updated with an equivalent based on AR4 results]*

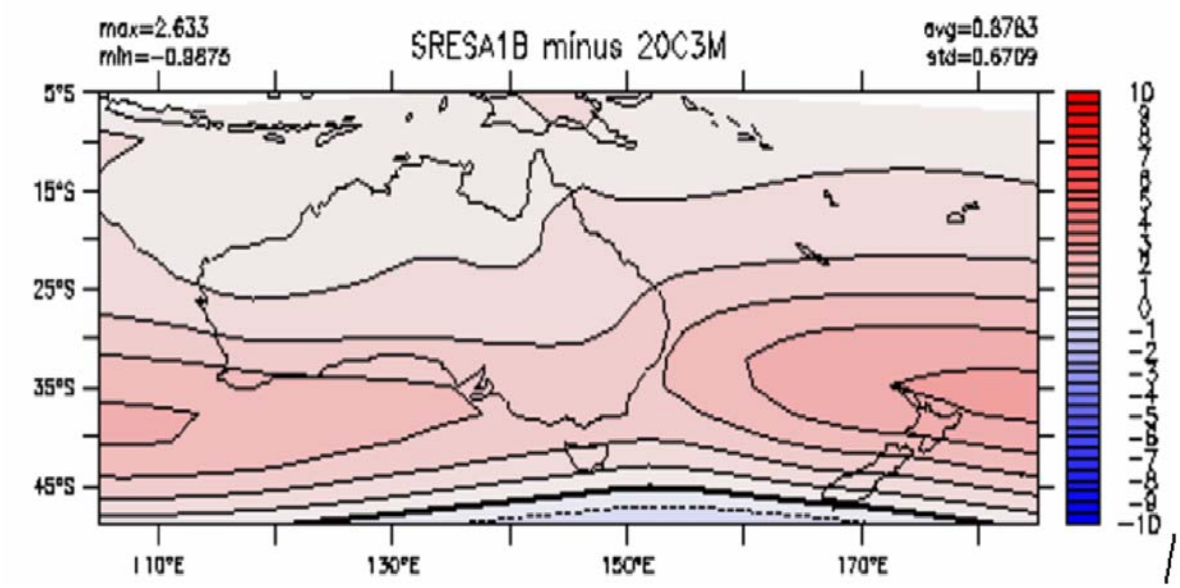

Figure 11.3.7.4. Ensemble mean change in sea level pressure between A1B and control in JJA in the AR4 simulations. Contour interval is 0.5 mb.

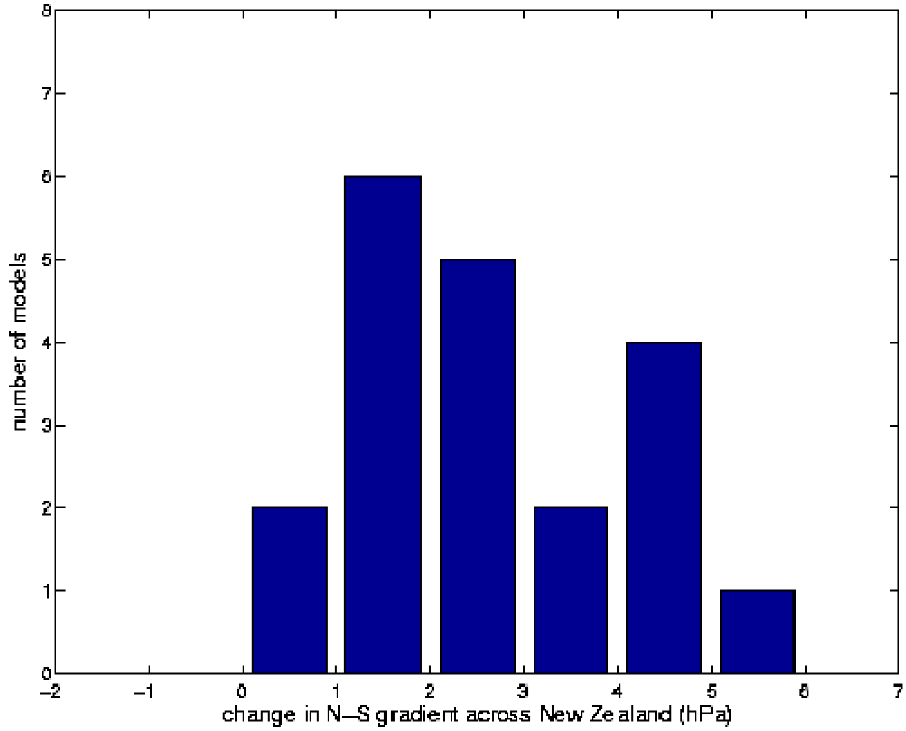

Figure 11.3.7.5. Change in the north-south pressure JJA gradient across New Zealand in the AR4 simulations.

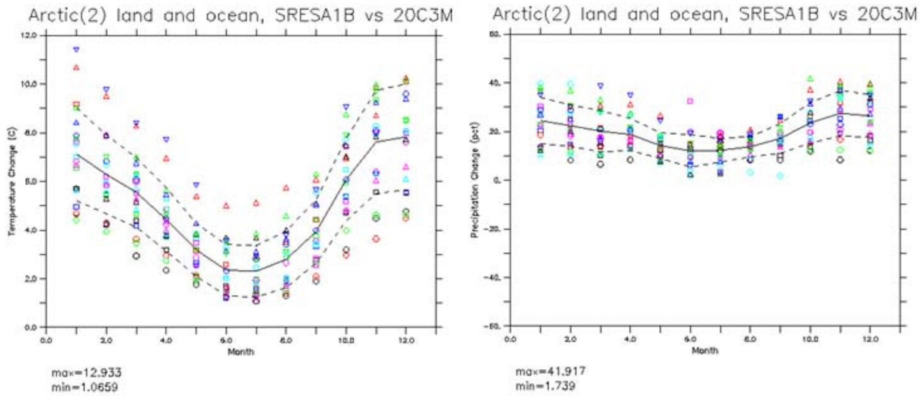

Figure 11.3.8.1. Annual cycle of monthly mean Arctic temperature and percentage precipitation changes (averaged over the area north of 60°N) (for 2079–2098 minus 1979–1998 under the A1B scenario). Solid lines are the AR4 model ensemble mean, dashed lines represent the one standard deviation across the different models, and the colored points are the individual model realizations.

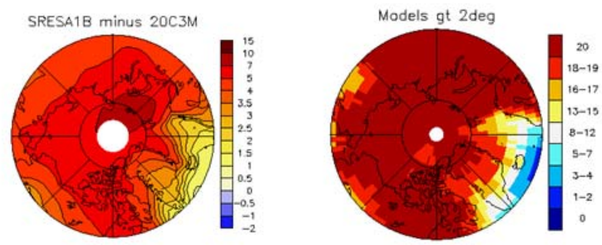

Figure 11.3.8.2. Annual surface temperature change (°C) from 1979–1998 to 2079–2098 in the Arctic under the A1B scenario. (a) mean over all 20 AR4 models, (b) number of AR4 models that generate a warming greater than 2°C.

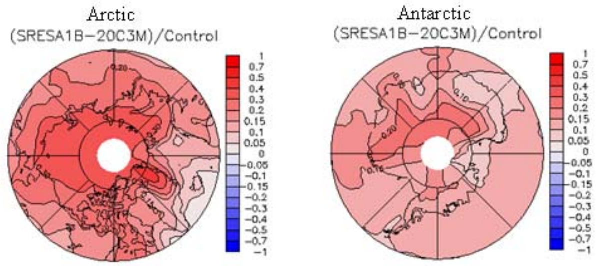

Figure 11.3.8.3. Annual percentage precipitation change from 1979–1998 to 2079–2098 in the Arctic and Antarctic under the A1B scenario (mean over all 20 AR4 models).

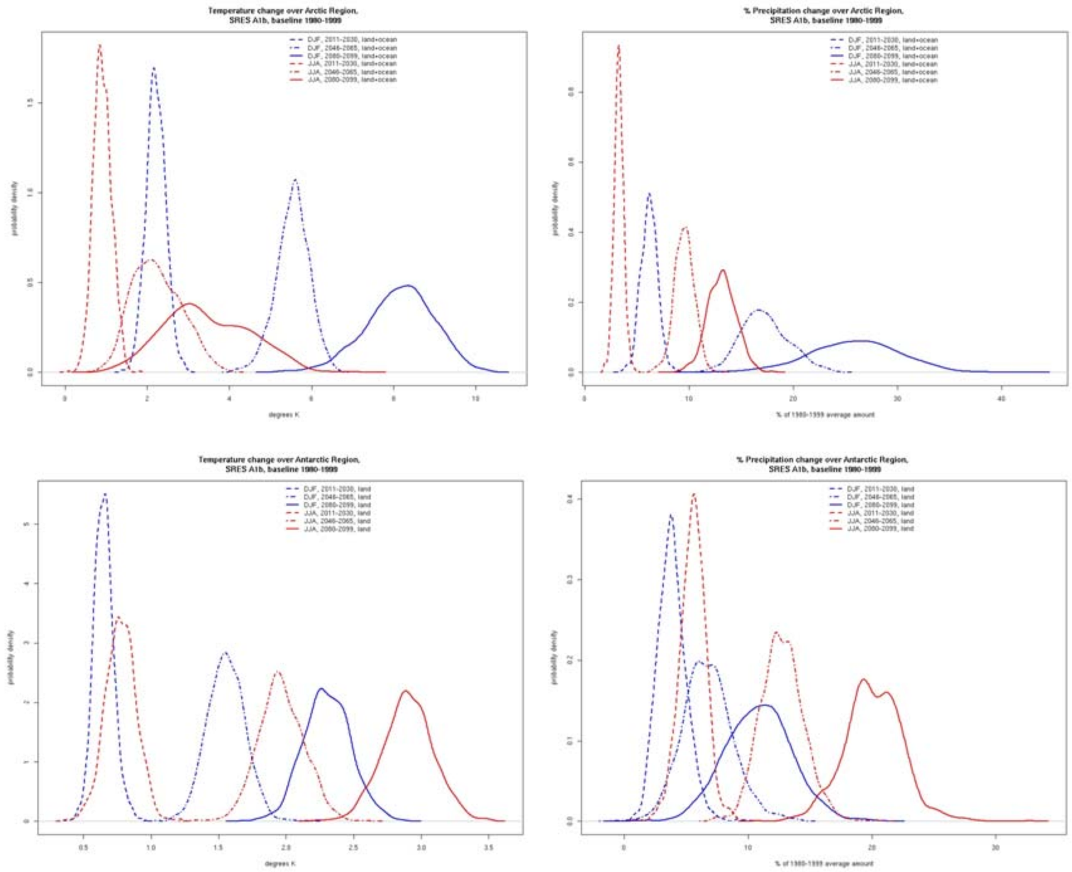

Figure 11.3.8.4. PDFs of winter and summer temperature and precipitation changes over the Arctic (averaged over the area north of 60°N) and the Antarctic continent (averaged over all land south of 60°S) for 2011–2030, 2046–2065, and 2080–2099 (baseline 1980–1999) under the A1B scenario. PDFs were calculated by the method of Tebaldi et al. (2005).

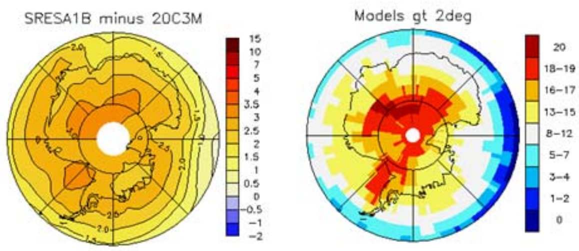

Figure 11.3.8.5. Annual surface temperature change (°C) from 1979–1998 to 2079–2098 in the Antarctic under the A1B scenario. (a) mean over all 20 AR4 models, (b) number of AR4 models that generate a warming greater than 2°C.

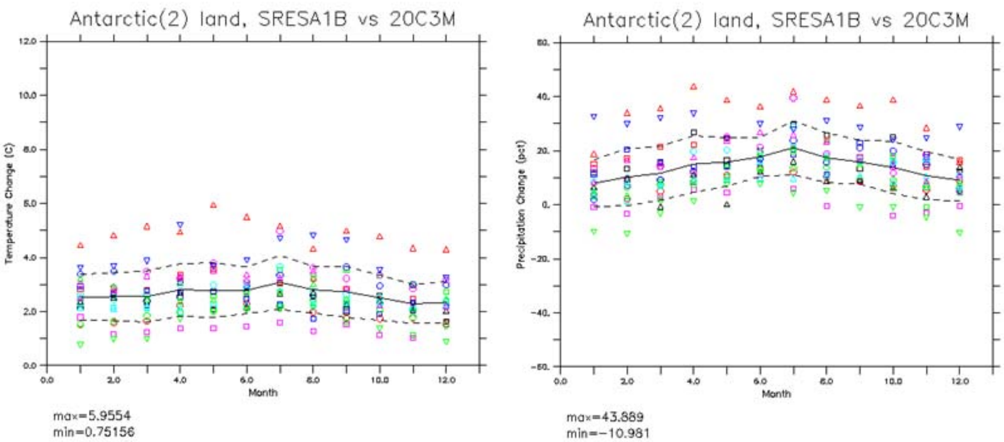

Figure 11.3.8.6. Annual cycle of monthly mean Antarctic temperature and percentage precipitation changes (averaged over the land area south of 60°N) (for 2079–2098 minus 1979–1998, under the A1B scenario). Solid lines are the AR4 model ensemble mean, dashed lines represent the one standard deviation across the different models, and the colored points are the individual model realizations.

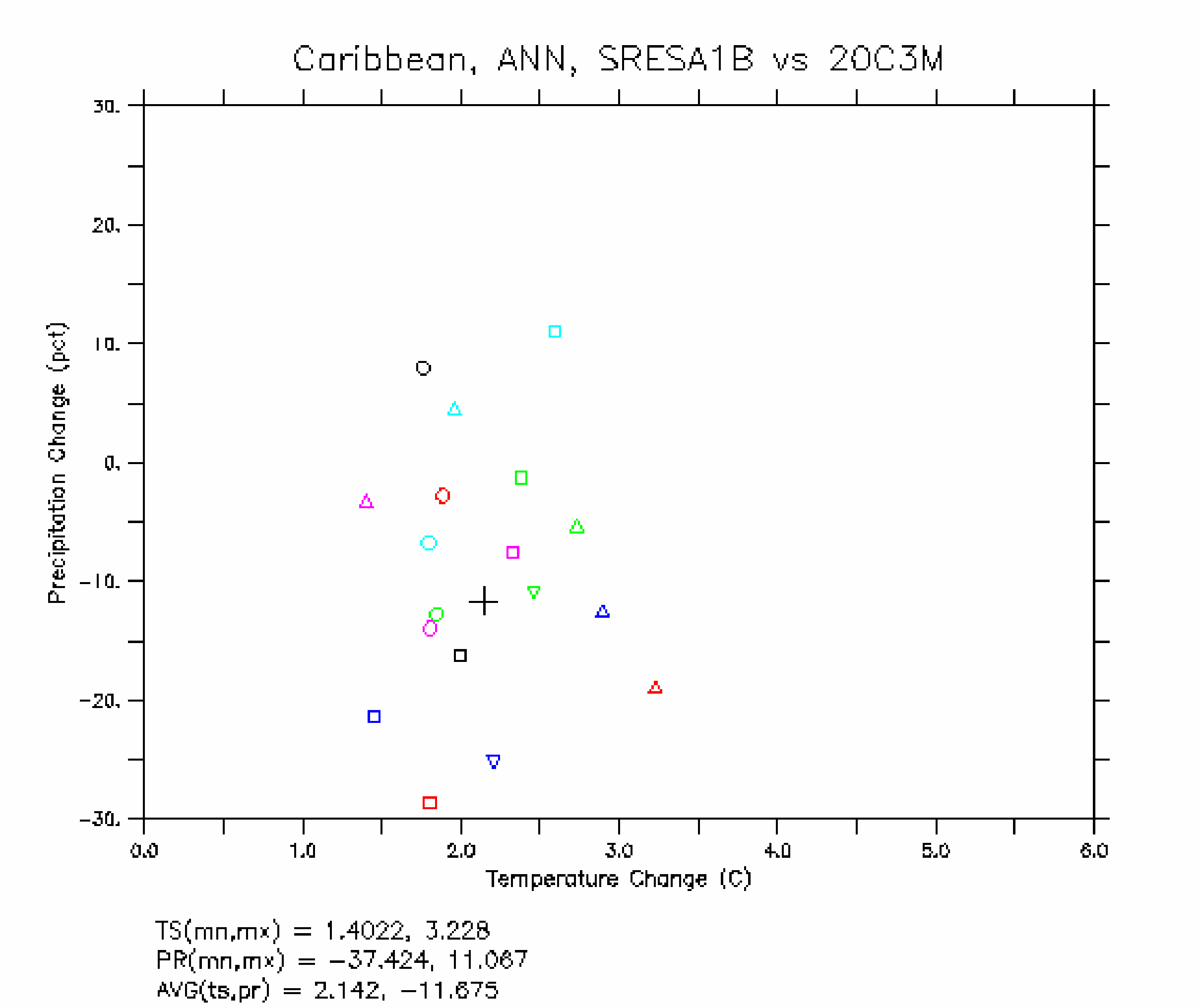

Figure 11.3.9.1. Precipitation change (%) vs temperature change (°C) from 1979–1988 to 2079–2098 obtained from 20 PCMDI models using the SRES A1B scenario for the Caribbean.

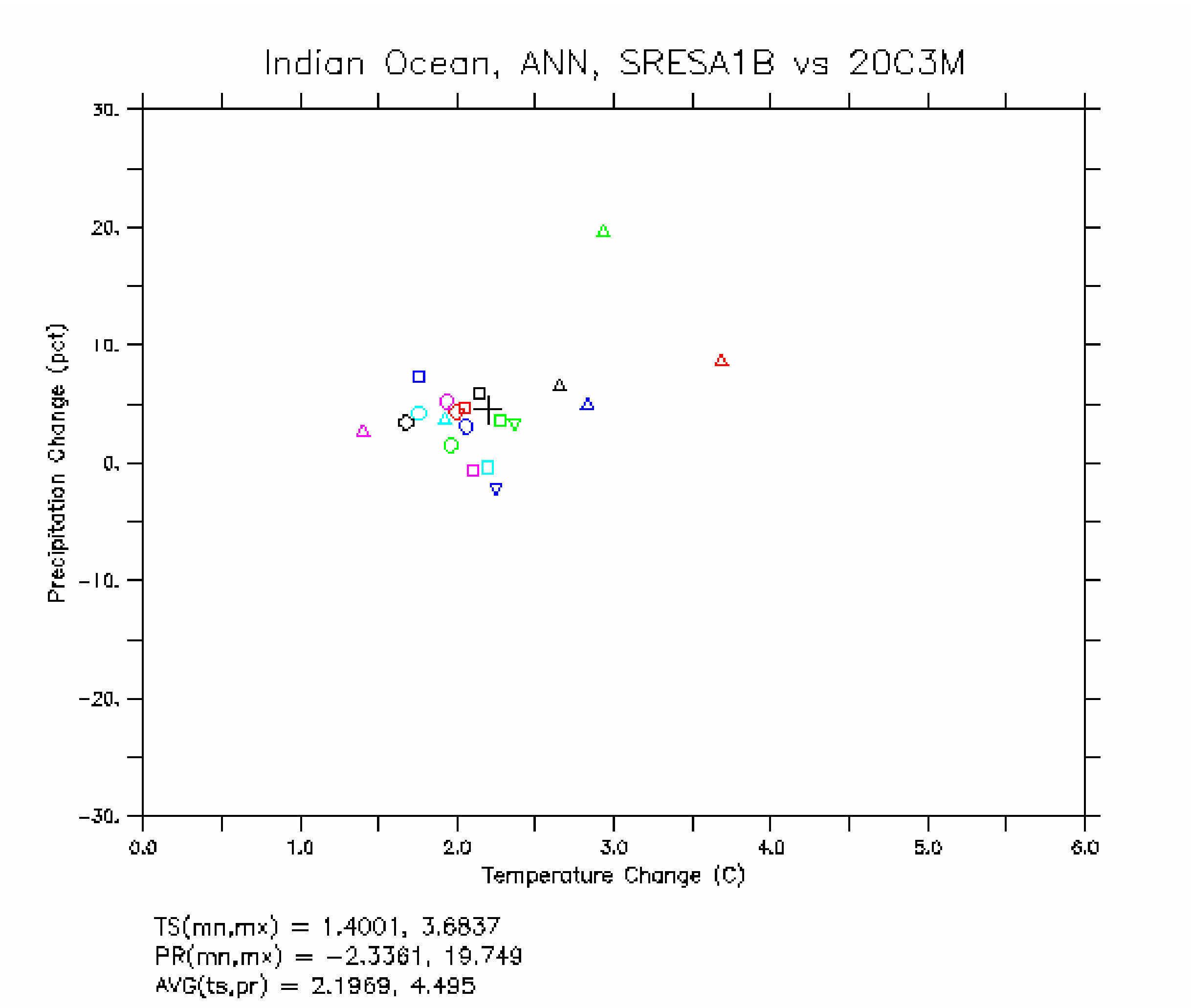

Figure 11.3.9.2. As for Figure 11.3.9.1 but for the Indian Ocean.

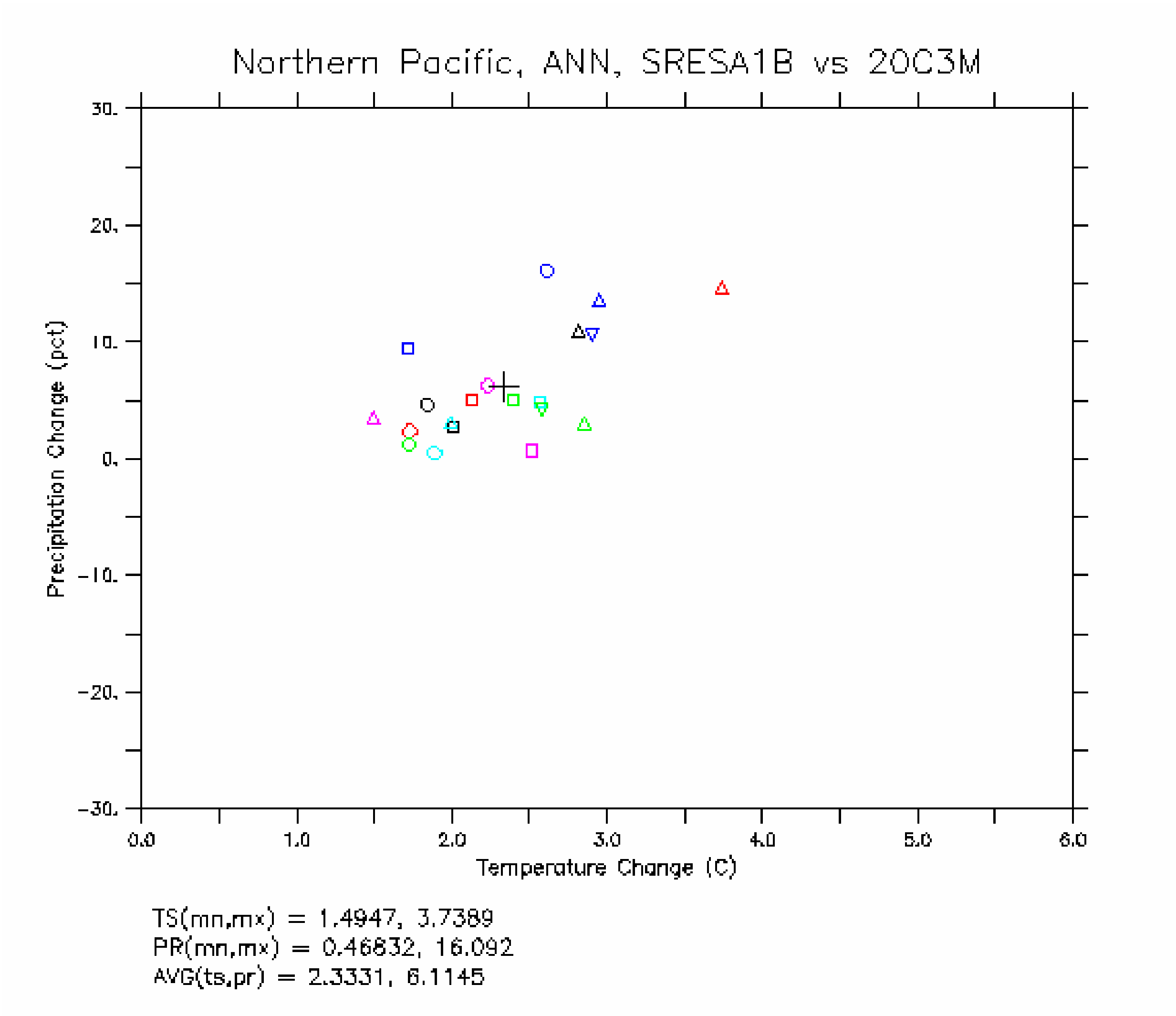

Figure 11.3.9.3. As for Figure 11.3.9.1 but for the Northern Pacific Ocean

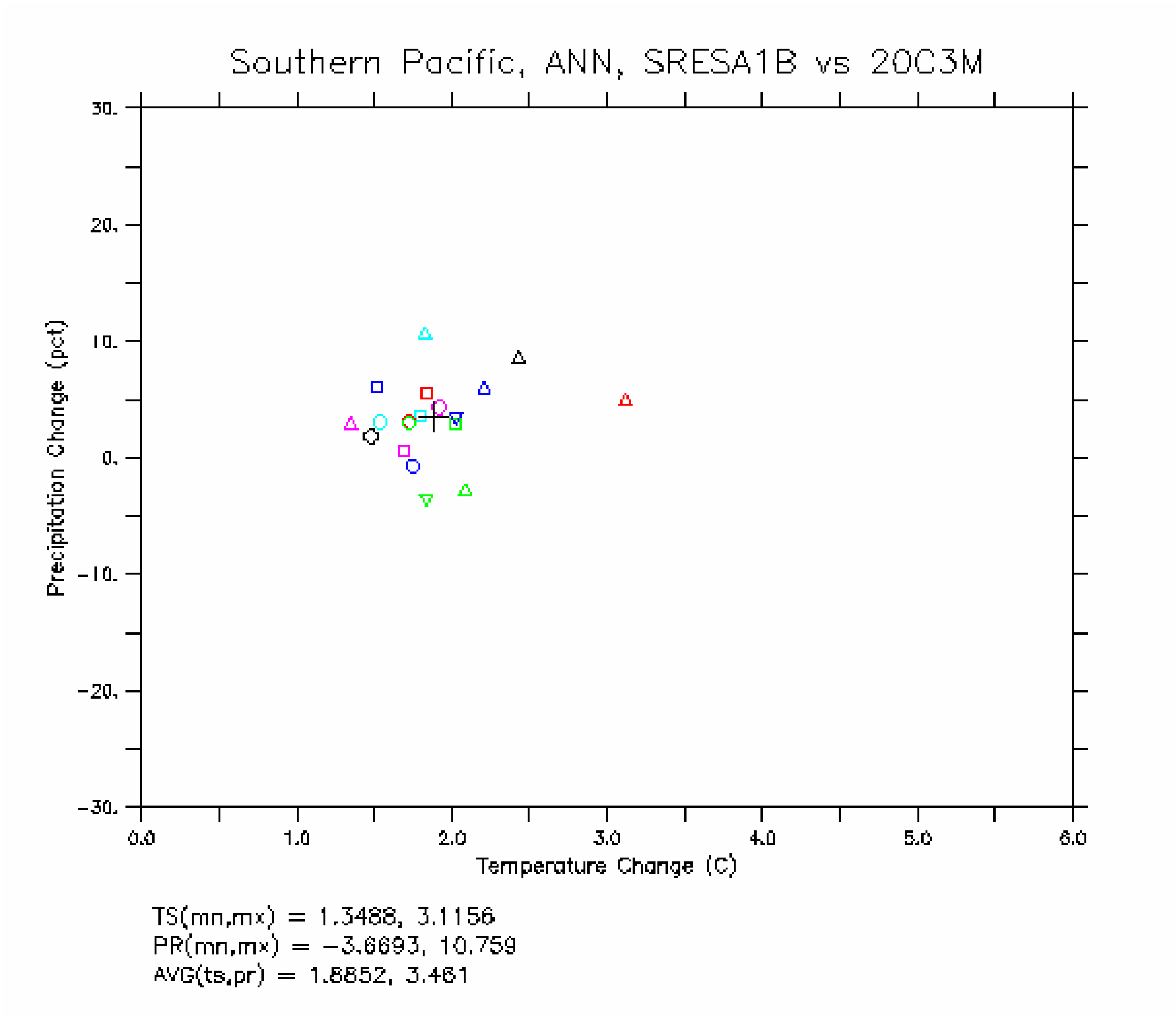

Figure 11.3.9.4. As for Figure 11.3.9.1 but for the Southern Pacific Ocean

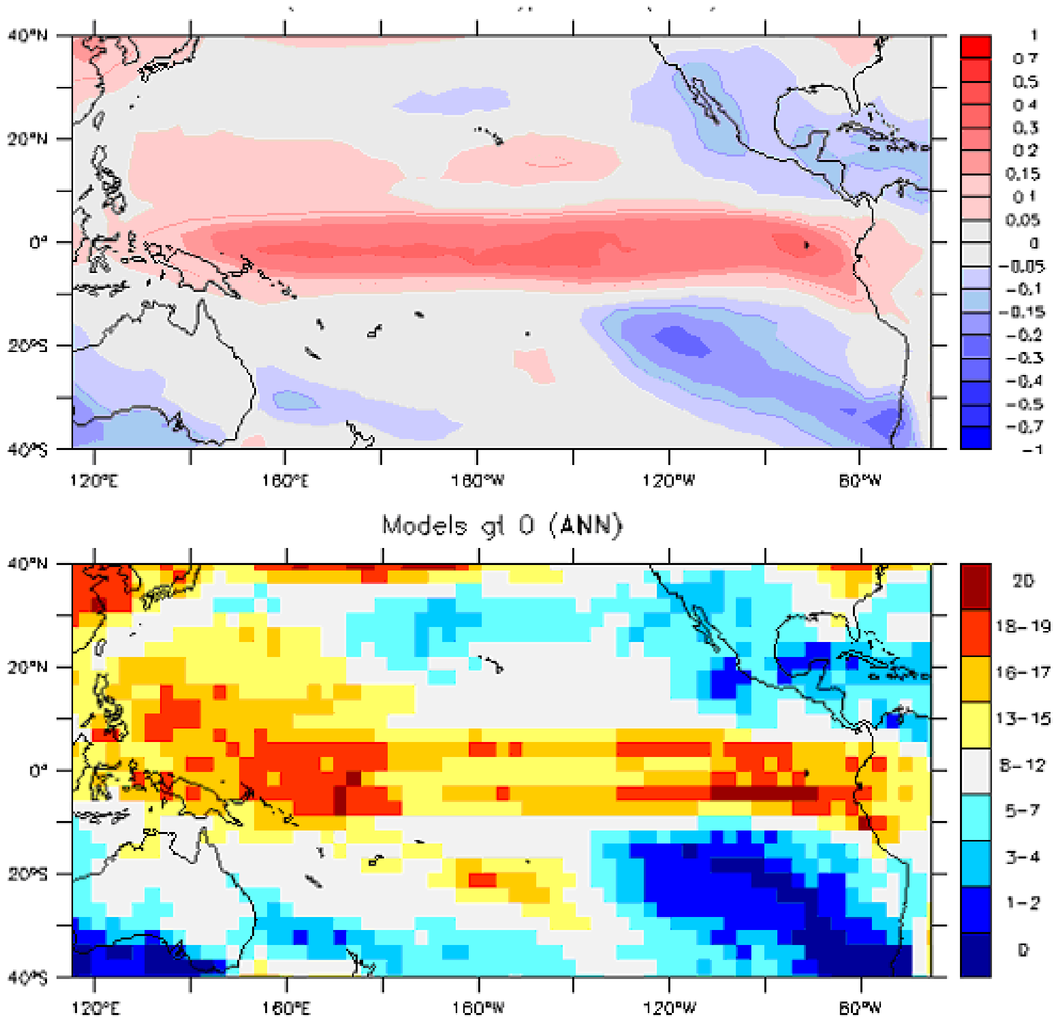

Figure 11.3.9.5. illustrates the spatial distribution of annual average rainfall change and inter-model consistency. It can be seen that the tendency for precipitation increase in the Pacific is strongest in the region of the ITCZ.

Box 11.1, Figure 1. [Placeholder: Map showing very likely and likely regional changes in mean and extremes]

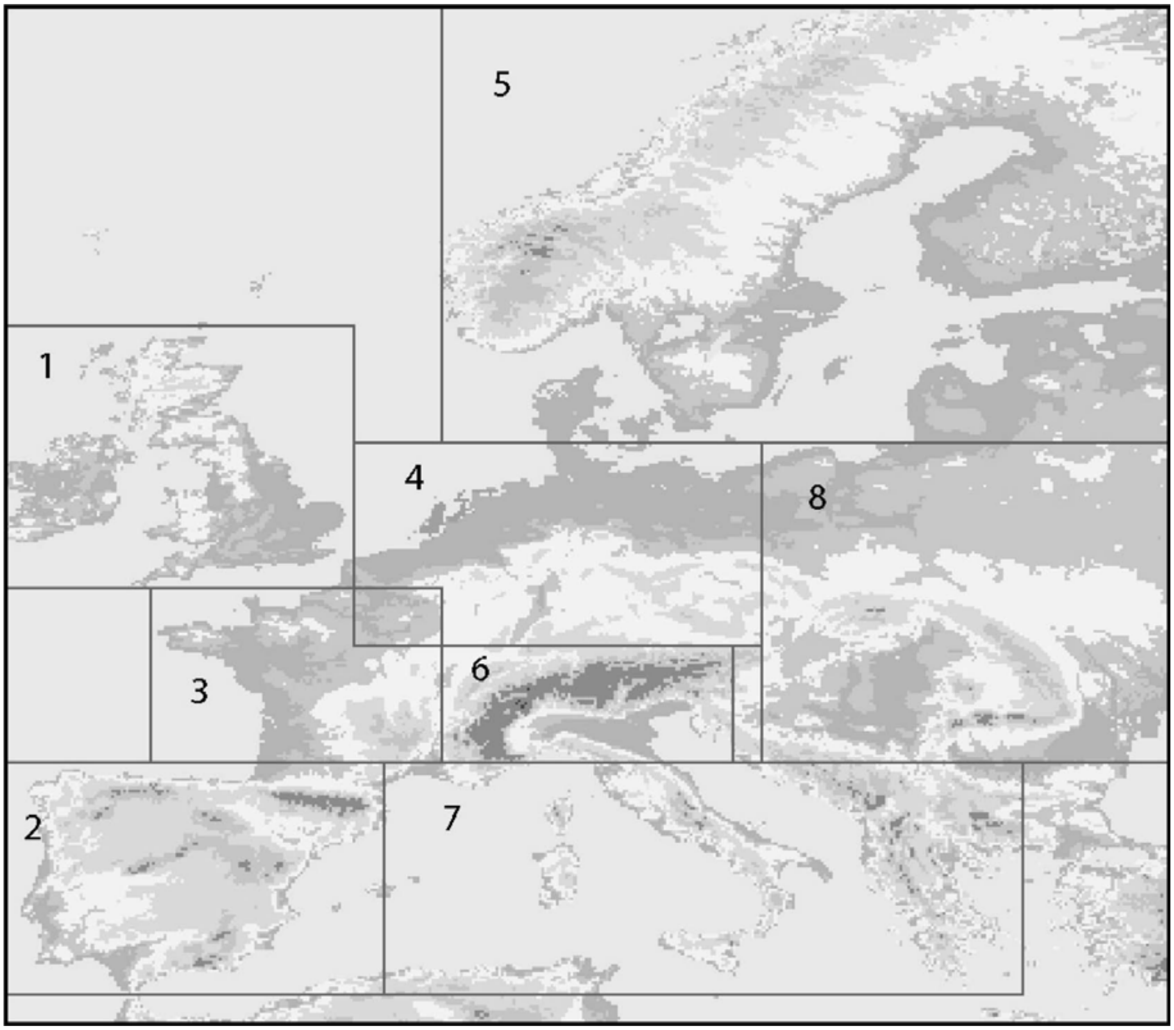

Box 11.2 Figure 1. PRUDENCE core region of interest. The eigth subdomains were used thoroughly for detailed analysis. (Déqué et al., 2005a)

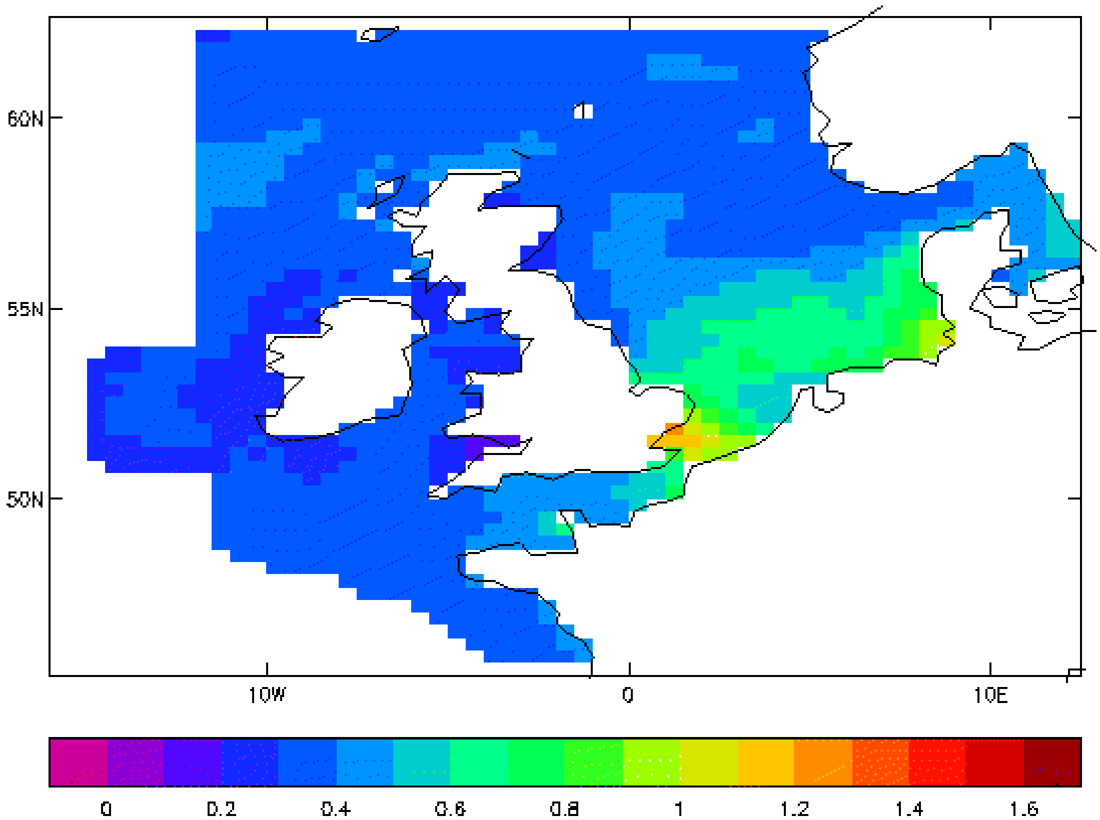

Box 11.4, Figure 1. Change the 50-year return period extreme water level due to changes in atmospheric storminess, mean sea level and vertical land movements (from Lowe and Gregory, 2005).